Microelectronic Cooling by Enhanced Pool Boiling of a Dielectric Fluorocarbon Liquid

T. M. Anderson
Graduate Research Assistant.

I. Mudawar
Associate Professor and Director.
Assoc. Mem. ASME

Boiling and Two-Phase Flow Laboratory,
School of Mechanical Engineering,
Purdue University,
West Lafayette, IN 47907

An experimental study of boiling heat transfer from a simulated microelectronic component immersed in a stagnant pool of the dielectric Fluorinert (FC-72) is presented. Various enhancement surfaces were attached to an electrically heated copper calorimeter bar having a vertically oriented heat transfer surface area of 12.7 × 12.7 mm². A number of enhancement schemes aimed at a reduction of the incipience temperature overshoot were tested, employing various arrangements of fins, studs, grooves, and vapor-trapping cavities. Atmospheric pressure testing revealed a variation in the magnitude of boiling curve incipience temperature excursion as a function of both macro- and microcharacterization of the surface geometry and initial conditions (pressure and temperature history) prior to boiling. Increased incipience temperatures accompanied prolonged periods of nonboiling. It is assumed that this is due to vapor embryos within surface cavities collapsing to smaller radii. Large artificially created cavities (0.3 mm diameter) were found incapable of maintaining a stable vapor embryo for time periods greater than 10 min. In comparison to flat surfaces, low-profile surface geometries having a structure scale of the order of one bubble departure diameter resulted in significant enhancement of nucleate boiling while drilled surfaces had minimal effectiveness. Surface finish and artificial cavities had no effect on CHF, but levels of critical heat flux computed on base area were strongly dependent on macrogeometry, due in part to increased surface area.

Introduction

Recent advances in the electronics industry have led to rapid miniaturization of integrated circuits. The past two decades have seen chip power densities increase by five orders of magnitude as integration technologies advanced to the VLSI level. Consequently, thermal design of more powerful cooling systems must be developed to allow chip dissipation to exceed the current 5 to 40 W/cm² limits.

The current cutting-edge high-power mainframe cooling technologies have already reached their upper performance limits imposed by the thermal resistance between the chip and the coolant. The Thermal Conduction Module (TCM) implemented in the IBM 3090 computer series, for example, utilizes indirect cooling of a large array of chips in a single module. Spring-loaded convex-tipped pistons conduct heat away from individual chips to a water-cooled cold plate. However, expected increases in mainframe computer chip power density may force indirect cooling methods to succumb to direct immersion cooling by dielectrics fluids such as the 3M Fluorinerts. Substitution of an intermediate boiling fluid between the chip and an enlarged cold plate (or condenser) would drastically reduce the internal thermal resistance compared to diffusion through a long and complex conduction path.

While recent studies by Tuckerman and Pease (1981) and Ramadhyani and Incropera (1987) are strong evidence of the cooling potential of single-phase forced convection, the accompanying linear relationship between heat duty and chip temperature makes it less attractive compared to nucleate boiling in the medium VLSI heat flux range (50–100 W/cm²). Pool boiling heat transfer tends to maintain the chip temperature within a narrow range while dissipating a wide range of heat fluxes. This pool boiling feature is very desirable in electronic cooling since chip temperatures are limited to 85°C. Additionally, forced convection systems are often plagued by the need for large pumps and complex plumbing.

Enhanced pool boiling of fluorocarbon liquids appears to be a promising first generation mainframe cooling technique for removal of large amounts of heat from individual chips. Independent gravity-driven thermosyphon modules (Fig. 1) may be able to cool arrays of high-power chips without the need for expensive pumps or complex plumbing. However, advances in the control of the often anomalous behavior of the boiling curve will be required before pool boiling heat

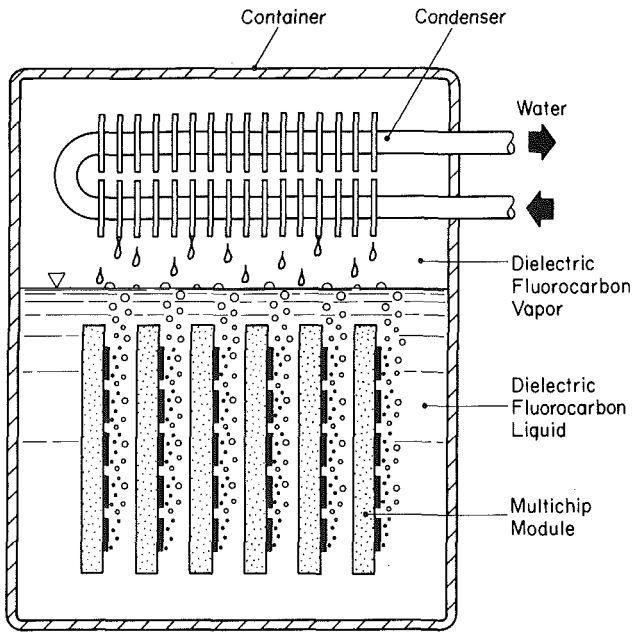

Fig. 1 Liquid-encapsulated gravity-driven thermosyphon cooling concept

Contributed by the Heat Transfer Division for publication in the JOURNAL OF HEAT TRANSFER. Manuscript received by the Heat Transfer Division March 11, 1988. Keywords: Boiling, Finned Surfaces, Phase-Change Phenomena.

transfer gains widespread popularity in the mainframe computer industry.

Presently much uncertainty exists in the prediction of the incipient boiling point. Flux levels corresponding to the cessation of boiling upon decreasing heat flux are usually much less than those encountered at the onset of boiling upon increasing heat flux. In other words, boiling incipience often occurs at temperatures much higher than expected and the excess superheat may quickly be dissipated by vigorous boiling resulting in potential damage to the heat source (chip) by thermal shock.

If a force balance is performed on a spherical bubble and it is assumed pressure is related to temperature by the Clausius–Clapeyron equation and that superheat is sufficiently small that $P_{sat} - T_{sat}$ linearity holds, then

$$\Delta T_i = \frac{T_{sat}\, v_{fg}}{h_{fg}} \frac{2\,\sigma}{r} \tag{1}$$

Equation (1) indicates that the superheat required to promote bubble growth and release is inversely proportional to the radius of the embryo within the cavity. Prevalent incipience theories (Hsu, 1962; Han and Griffith, 1965; Davis and Anderson, 1966) assume the smallest value of bubble radius (and therefore the greatest superheat) is equal or proportional to the radius of the cavity r_{cav}. Following this assumption the wall superheat necessary to cause boiling is determined by cavity size distribution on the boiling surface. But for the special case of dielectric fluorocarbons, the extremely low contact angle causes almost complete liquid flooding of surface cavities, leaving very small vapor embryos. These embryos require much higher superheat than predicted by equation (1) based on cavity radius (Bar-Cohen and Simon, 1986). Hence the key to estimation of the boiling incipience temperature for very wetting fluids lies in prediction of the distribution of embryo sizes rather than solely on the specification of surface characteristics.

The rapid temperature drop that often accompanies boiling incipience is a product of the large and rapid change in the heat transfer coefficient as the heat transfer mode shifts from natural convection to nucleate boiling. For a small fairly isothermal heat transfer surface undergoing both natural convection and boiling on separate areas, A_{nc} and A_b, the total heat load is comprised of a combination of natural convection and boiling components. That is,

$$\frac{qA}{\Delta T_{sat}} = h\,A = h_{nc}\,A_{nc} + h_b\,A_b \tag{2}$$

where h_{nc} and h_b are the heat transfer coefficients for natural convection and boiling, respectively. Defining the boiling area fraction as $A^* = A_b/A$

$$h = h_{nc}(1 - A^*) + h_b A^* \tag{3}$$

As A^* grows gradually toward unity in equation (3), the heat transfer coefficient h will likewise increase smoothly to the value of h_b.

The behavior of A^* with respect to time can be influenced by the size of the heat transfer surface and the pattern of boiling activation. Small heaters are often subject to large jumps in A^* since the area that is influenced by the boiling of a single site is a significant fraction of heater area. Rapid patterns of activation force large swings in A^* and therefore result in considerable incipience excursion. Blander and Katz (1975), Marto and Lepere (1982), and Hui and Thome (1985) reported explosive activation of boiling sites and considerable incipience temperature drop.

Conduction effects within the test heater can greatly influence the magnitude of the detected incipience excursion. Foil heaters such as those used by Park and Bergles (1986) allow little conduction along the heat transfer surface. Consequently, temperature measurements on these heaters are strongly affected by only a small localized area of the surface (smaller than the total heat surface area). The large change in the local heat transfer coefficient is sensed as a relatively large temperature fallback. Thick heaters, such as those of the present study, allow conduction within the heat transfer surface, which dampens the localized effect of the activation of a few boiling sites. Rapid activation of the entire surface may still result in incipience excursion but thermal shock is damped by the increased thermal capacitance.

The purpose of this study is to determine the effect of some types of surface roughness scheme and surface structure on pool boiling incipience, nucleate boiling, and critical heat flux (CHF) using FC-72 dielectric fluorocarbon liquid. Low-profile enhancements built upon a 12.7×12.7 mm^2 vertical surface were studied with flow visualization employed to facilitate interpretation of results.

Experimental Methods

A highly instrumented pool boiling facility was developed to simulate the microelectronic boiling module environment. A schematic of the power supply, data acquisition, test and charging vessels, and supporting plumbing in shown in Fig. 2. To maintain fluid purity, only stainless steel and fluorocarbon compatible materials were in direct contact with the working fluid. Leaks in the test chamber were detected by repeated application of vacuum and pressure and completely sealed.

A stainless steel pressure vessel rated for 22 bars at 200°C with three access nozzles was utilized as the test chamber. For optical access, quartz sight glass window flanges capped two of the access ports while the heater module was mounted through the third. The bulk of the natural convection heat loss from the vessel to the ambient was compensated by large flexible band heaters wrapped around the vessel. To maintain

Nomenclature

$A^* = A_b/A$
A = total heat transfer area
A_b = boiling fraction of total area
A_{nc} = natural convection fraction of total area
g = acceleration due to gravity
H = heater height
h = average heat transfer coefficient $= q/\Delta T_{sat}$
h_b = boiling heat transfer coefficient
h_{fg} = latent heat of vaporization
h_{nc} = natural convection heat transfer coefficient
k = thermal conductivity of liquid
Nu_c = Nusselt number at center of foil heaters $= h_{nc}H/2k$
P = pressure
q = heat flux
r = bubble radius
r_{cav} = cavity radius
Ra_c^* = modified Rayleigh number at center of foil heaters $= g\beta qH^4/(16k\nu\alpha)$
Δt^* = nonboiling time interval between boiling states
ΔT_h = incipient boiling temperature excursion
ΔT_i = incipient boiling superheat temperature
ΔT_{sat} = wall superheat $= (T_w - T_{sat})$
T_{sat} = saturation temperature
T_w = temperature of heater surface or fin base
v_{fg} = latent specific volume change
W = heater width
α = thermal diffusivity of liquid
β = coefficient of expansion of liquid
ν = kinematic viscosity of liquid
σ = surface tension

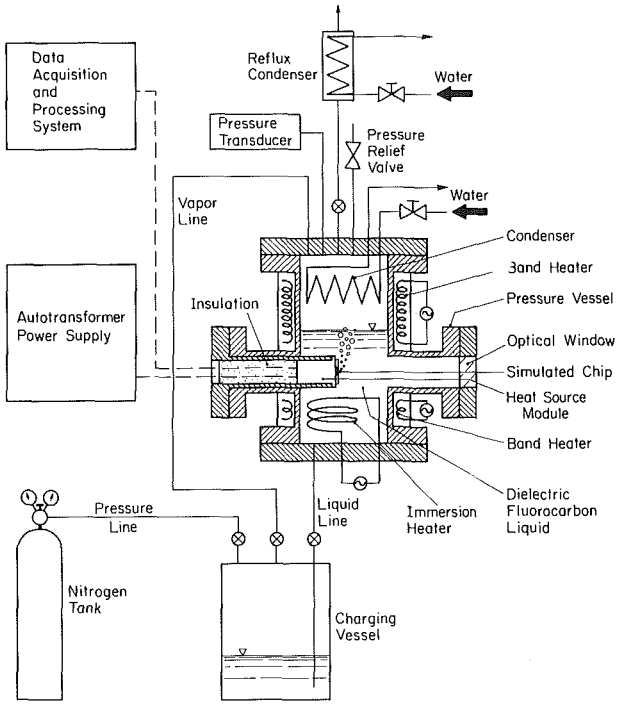

Fig. 2 Schematic of pool boiling facility

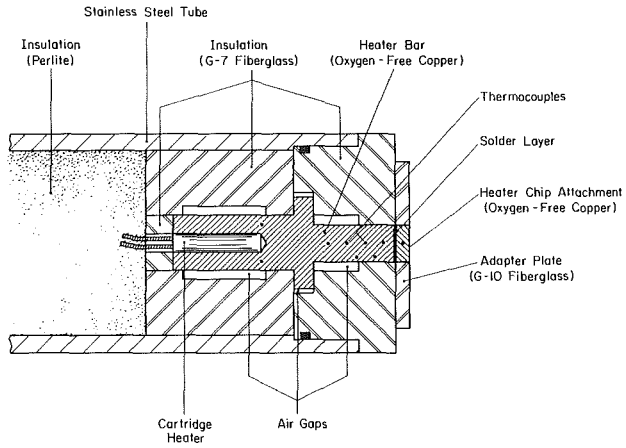

Fig. 3 Sectional diagram of the heat source module

precise control of the temperature and pressure a temperature controller powered an immersion heater located in the liquid pool near the base of the vessel. The bulk fluid temperature was measured by a set of type K thermocouples located below the test surface. Heat was removed from the vessel via a water-cooled condenser coiled within the upper section of the vessel. Combined use of the immersion heater and condenser allowed maintaining the fluid at atmospheric saturated conditions.

Between test runs the test fluid was stored in a charging vessel below the test section. Dry high-pressure nitrogen was employed to drive the stored liquid into the test chamber prior to each test. Deaeration of the fluid to remove entrained gases was performed within the test vessel by vigorous boiling for 30 min. The reflux condenser above the vessel recovered escaping FC-72 vapor and returned it directly to the test vessel. Danielson et al. (1987) employed a gas chromatographic technique to evaluate the effectiveness of this deaeration procedure on a similar system and found the residual air concentration to be less than 1 percent by volume after 3 min of degassing.

The heat source module, similar to those used by Nakayama et al. (1984) and Park and Bergles (1985), was fabricated from a copper bar, cartridge heater, two G-7 insulating plates, and a mounting tube as shown in Fig. 3. An oxygen-free copper assembly was employed to conduct heat from a Watlow cartridge heater through a calorimeter bar section and into the simulated chip attachment. Insulation and positioning of the copper bar were accomplished by a G-7 fiberglass plastic cap and collar arrangement. The interface between the bar and insulation was sealed with high-temperature silicone RTV. The G-7 cap was fitted within the stainless mounting tube using a Viton O-ring and held against the test vessel pressure by set screws.

Heat flux through the test surface was determined by a combination of electrical and thermal measurements. Power supplied to the cartridge heater by a 0–140 V autotransformer was measured by a Scientific Colombus Exceltronic Watt transducer to determine an electrical flux value within ±0.1 percent uncorrected for heat loss. Four electrically insulated 0.075 mm chromel-alumel wire thermocouples spaced 3.18 mm apart were used to determine the thermal heat flux through the calorimeter section of the copper bar by assuming one-dimensional heat conduction. The thermal conductivity of the copper was 391 W/m•K (±1.2 percent) as determined by the supplier. It was found that a least-squares parabolic fit of the four temperatures showed little nonlinearity. This result confirmed both the low level of heat loss and the validity of the one-dimensional heat flow assumption.

Plotting the percent heat loss (defined as the percent difference between the electrical and thermal flux) versus the electrical power input revealed a smooth function of heat loss with electric power. The low power region of the plot was somewhat scattered due to the limited resoluton of the thermocouples (±0.05°C). These random round-off errors were eliminated by fitting a curve through the data. The empirically derived relationship was then used to correct the electrical flux for heat loss. Thus, the heat flux data presented in this paper correspond to the *thermal flux* corrected only for thermocouple round-off errors. This procedure was utilized for each boiling curve since heat loss is a sensitive function of the detailed boundary conditions of the heater.

Several test conditions were repeated to verify the reproducibility of the data and validate the experimental technique. The variation in data sets was within ±0.05°C at heat fluxes smaller than 1 W/cm^2 and within ±0.1°C at higher heat fluxes.

Enhanced surface boiling chips were directly soldered to the heat source module. An adapter plate was fitted around the chip to provide a surface flush with the face of the chip and to insulate the chip sides. A relatively low temperature (180°C) lead/tin solder gave the best combination of strength, thermal conductivity, and operating temperature range for chip attachment. The thermal capacitance of the heater created a short time delay between the development of the vapor blanket at CHF and the temperature rise at the bond area. This delay allowed the operator to shut off power to the heater prior to melting of the solder.

All augmentation schemes were built upon a standard 4.78-mm-thick base chip with an area of 12.7×12.7 mm^2. A 0.075 mm wire type K thermocouple implanted in the center of the attachment was used to extrapolate an average surface temperature and evaluate the bond effectiveness. Experiments with multiple thermocouples within the chip confirmed numerical predictions that the central location of a single thermocouple bead well represented the average reference base surface temperature.

Three categories of enhanced surfaces were tested: smooth, drilled, and low-profile structures. Geometries were chosen on the basis of simplicity and repeatability, requiring only existing manufacturing technology. Three smooth surfaces were

examined to contrast the effects of surface roughness. A mirror finish was prepared by buffing a milled surface with 12,000 grit lapping compound. A similarly prepared mirror smooth surface was roughened by longitudinal sanding with a 600 grit silicon wet/dry sandpaper to investigate the impact of microscopic grooving of the surface. Examination of the sanded surface under a scanning electron microscope revealed the dense pattern of parallel 0.6–1.0 μm gouges (or scratches) shown in Fig. 4(a). The micrograph also shows a void within the copper that was exposed by machining. Surfaces marred by such void anomalies were not used for testing.

The seemingly random dendritic structure of Fig. 4(b) was the result of vapor blasting a water-base slurry of 12,000 grit silica particles onto a mirror polished surface by means of compressed air. Vapor blasting appears to replace any prior surface roughness such as marks left by polishing or sanding with a homogeneous structure having an effective pore size near 15 μm as determined by the ASTM F-316-80 testing procedure using a Coulter porometer. Cavity size distribution was determined by submerging the surface in a given mass of pressurized liquid and measuring the displacement of liquid toward the surface as more cavities were intruded with liquid with increasing pressure. All drilled and low-profile surfaces were vapor blasted to eliminate variations in surface finish.

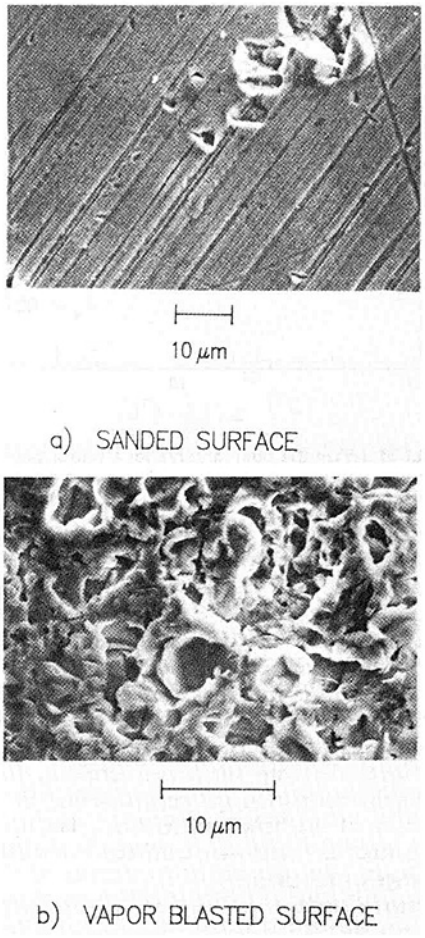

Fig. 4 Scanning electron microscope photographs of surface roughness

The effect of artificial cavities was examined using the three surfaces shown in Fig. 5. A uniform cavity pattern of seventeen 0.36-mm-dia holes on 0.72-mm centers was drilled into a vapor-blasted chip to simulate shallow 0.41-mm-deep artificial cavities. In an attempt to use gravity to aid retention of a stable vapor embryo, the holes of the inclined drill augmentation form a 30-deg angle with the surface.

Three low-profile enhancement structures were used in this study (Fig. 6). The microfin surface was characterized by twenty 0.305-mm-wide vertical fins of 0.508-mm length separated on 0.610-mm centers. This design was based on the enhanced surface geometries of Nakayama et al. (1984). The microstud geometry was formed by modifying a microfin surface with horizontal cross-cuts. Similar in concept to the inclined drill surface, the inclined microgroove was fabricated in an attempt to trap vapor pockets within nine grooves oriented at 30-deg angle to gravity.

The time, temperature, and pressure history prior to boiling was found to be the primary factor affecting the magnitude of incipient boiling hysteresis. To allow comparison of the hysteresis behavior of the various enhanced surfaces, a standardized test procedure was required. Unless otherwise noted, the presented data resulted from the following procedure:

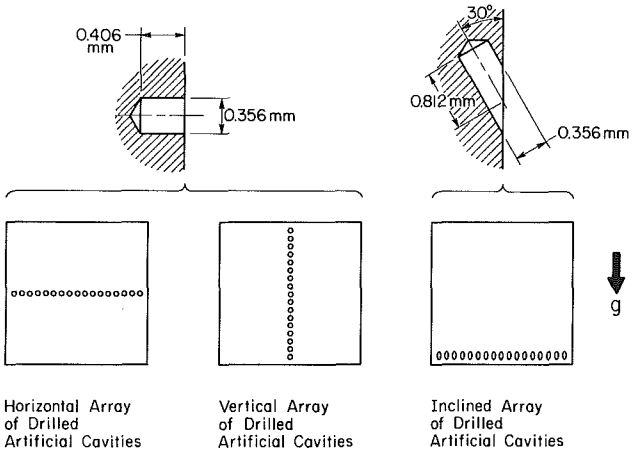

Fig. 5 Artificial cavity configurations

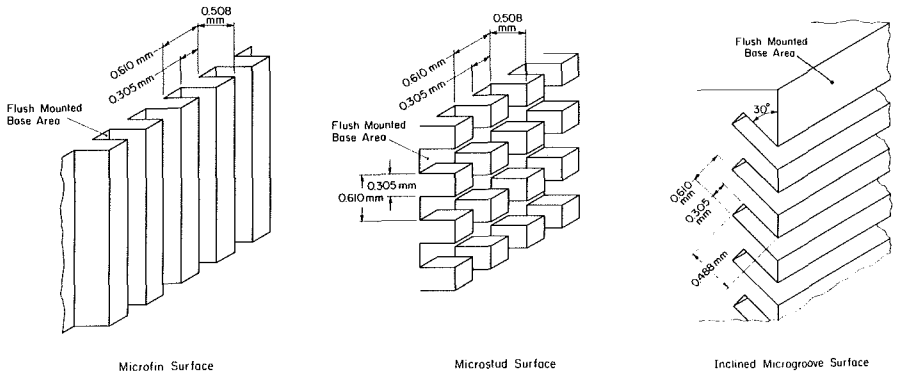

Fig. 6 Low-profile enhancement structures

1 The test chamber was charged then deaerted by 30 min of vigorous boiling at the immersion heater and test surface.

2 The system was closed and the immersion heater brought back to a nonboiling mode to maintain saturated conditions.

3 The test heater was shut off and the system allowed to stabilize for $\Delta t^* = 8$ h.

4 Power was supplied to the test heater in small increments.

5 The test continued to the critical heat flux condition or once within the fully developed region, the power to the heater was gradually decreased, and after waiting at the zero power level for $\Delta t^* = 10$ min, power was again increased toward CHF. The CHF condition was defined by the event where a small increment in power resulted in a rapid and large temperature rise as a film boiling mode was approached. The highest stable heat flux condition attainable prior to this event was designated to be the CHF point.

Results and Discussion

The influences of Δt^*, surface roughness, artificial cavities, and low-profile structures were examined for pool boiling of FC-72 on a vertical surface at atmospheric pressure. The data are presented in the form of heat flux versus wall superheat to allow comparison of such performance parameters as the natural convection heat transfer coefficient, incipience temperature, magnitude of incipience excursion, growth pattern of the boiling region, enhancement of nucleate boiling, and critical heat flux.

Effects of Nonboiling Waiting Period. The results of variations in Δt^*, the nonboiling time interval, were studied with the mirror polished surface to minimize the dependence on surface characteristics. Figure 7 shows natural convection heat transfer was unaffected by the nonboiling time interval, but as Δt^* was increased from 8 to 19 and 72 h, the boiling incipience temperature ΔT_i rose from 15.0 to 23.1 and 30.6°C, respectively. The authors suggest this variation indicates a dependence of boiling incipience on embryo size rather than cavity size for highly wetting fluids such as FC-72. Considering a decreasing flux situation, after an active cavity ceases boiling the vapor embryo shifts from a growth process into a collapsing mode as the vapor condenses into the surrounding liquid. As time progresses, the embryo radius decreases, thereby requiring a greater superheat to resume growing and re-initiate boiling. The data of Marto and Lepere (1982) also indicate the dependence of ΔT_i on the preboiling history. Sabersky and Gates (1955) examined the effect of an embryo-collapsing pressurization treatment and found high incipience temperatures resulted from shrunken vapor embryos.

The magnitude of incipience excursion detected for $\Delta t^* = 8$ and 19 h was less than 1°C but increased to greater than 10°C when the vapor embryos were allowed to shrink for 72 h. Visual observation of the growth patterns of the boiling patch revealed the correlation between the preboiling history with the time rate of change of the boiling area fraction A^*, the incipience superheat ΔT_i, and the incipience excursion ΔT_h. It is proposed that for shorter Δt^* insufficient condensation of the vapor into liquid caused little collapse of vapor embryos, thus allowing initial boiling to begin at modest surface superheat. The total heat transfer was adequately enhanced at the onset of boiling to stabilize the growth of A^*, resulting in gradual departure from the natural convection regime as the initial bubble nucleation front near the top edge of the heater spread slowly downward in response to increasing heat load. On the other hand, the average surface temperature for the longest condensation time examined, $\Delta t^* = 72$, was elevated beyond the $T_w = 85$°C electronic chip junction temperature limit to a point where a chain reaction of activation took place as boiling sites triggered nucleation at neighboring sites in rapid succession. The boiling region spread over approximately 45 percent of the surface within a few milliseconds, consistent with Marto and Lepere's observations of rapid activation on cylindrical commercial surfaces. The number of active sites dropped fourfold as the 10.4°C of excess superheat was reduced by a few seconds of vigorous boiling. The effect of the location of the active sites is evidenced by comparing the $\Delta t^* = 8$ and 19 h curves with the $\Delta t^* = 72$ h curve. Over the 3.5 to 6 W/cm² range of heat flux the $\Delta t^* = 72$ h curve shows marked enhancement because the active boiling sites are well distributed over the chip surface. Therefore, fluid mixing caused by bubble formation and departure may be influencing a large portion of the heat transfer area. The active boiling sites for the other Δt^* tests were confined to a small area near the upper edge of the chip.

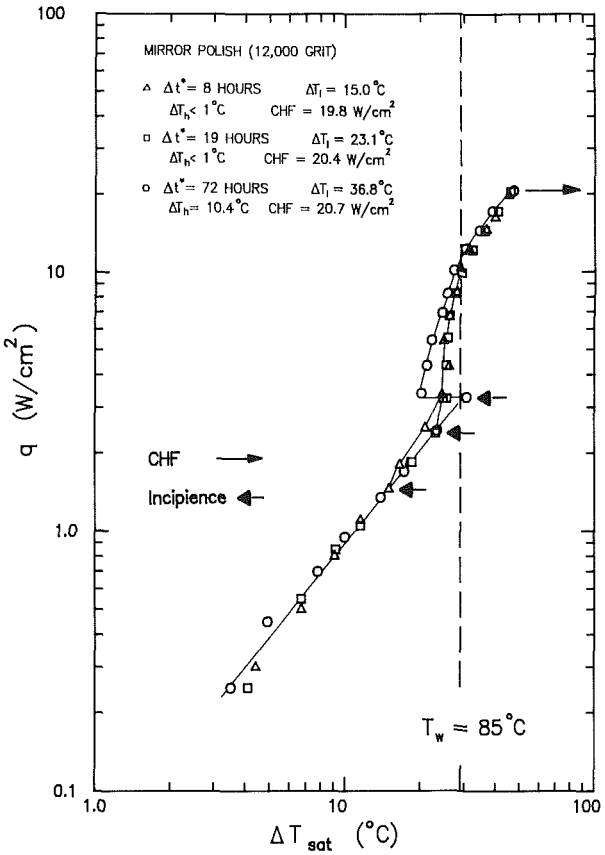

Fig. 7 Effect of Δt^* on the boiling curve for a mirror polished surface

As the mirror surface tests neared fully developed boiling ($q \approx 8$ W/cm²) the boiling curves converged indicating Δt^* affects the boiling performance only in the partially developed nucleate boiling regime. Similarly, identical CHF values were obtained for the three tests.

To facilitate comparison to subsequent tests, it should be noted that the nucleate boiling portion of these curves lay relatively close to the $T_w = 85$°C line and the heat fluxes at that temperature were only half of the peak values.

A strong argument against extending incipience theories based on cavity radius r_{cav} to fluids having very low contact angles can be built upon these incipience results since calculation of ΔT_i based on r_{cav} would predict equal incipience temperature values for each of the three cases shown in Fig. 8.

Effects of Surface Roughness. Surfaces can be characterized on a microscopic scale by determining the effect of roughness on boiling parameters. Comparing the mirror polished, sanded, and vapor blasted enhancements reveals a dependence of incipience temperature, incipience excursion, and nucleate boiling on microcharacteristics of the surface tex-

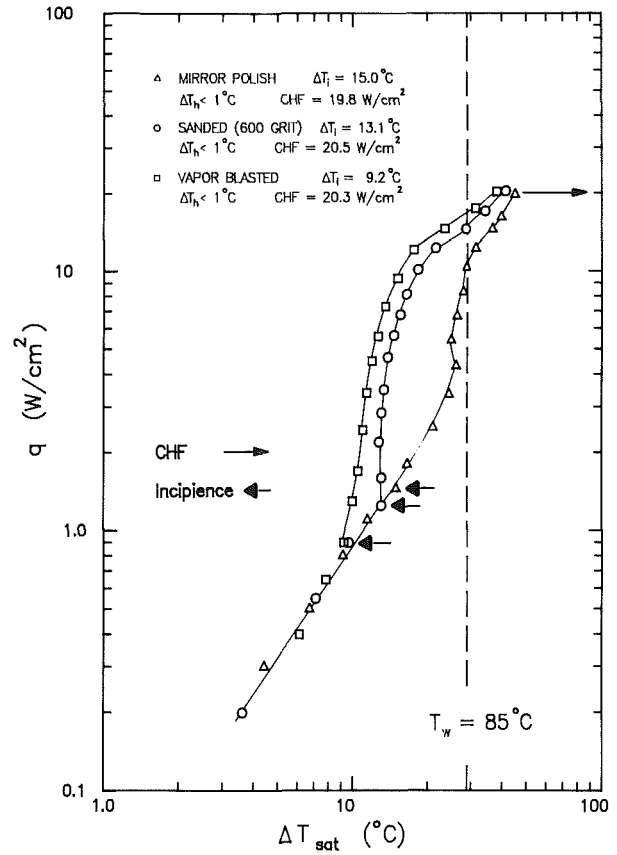

Fig. 8 Effect of surface roughness on the boiling curve for a flat vertical surface

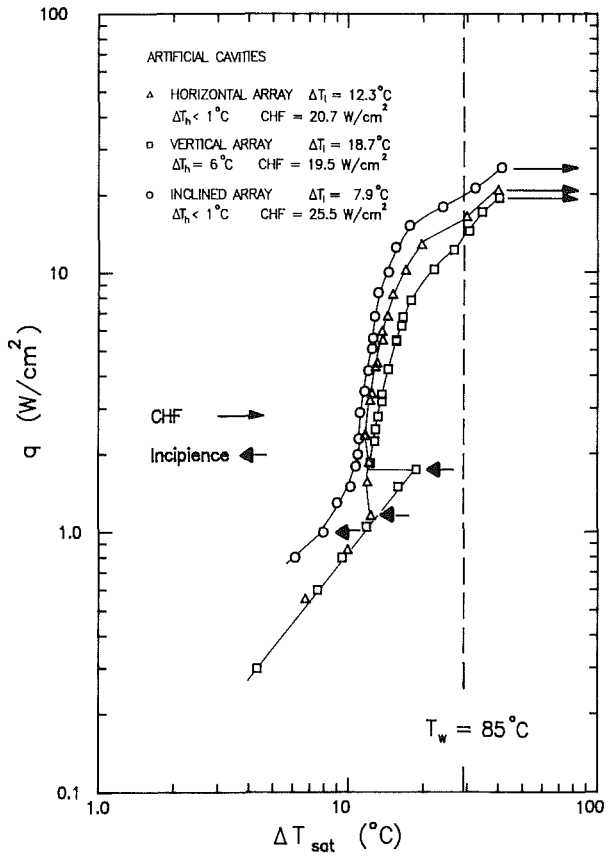

Fig. 9 Effect of artificial cavities on the boiling curve for a flat vertical surface

ture (Fig. 8). Contrasting the single-phase results suggests little effect of microroughness on natural convection; however, subject to equivalent initial conditions, increasing roughness promoted earlier incipience and therefore reduced incipience excursion. The depression of the vapor blasted surface incipience temperature is assumed to be evidence of a connection to embryo stability since within the distribution of the complex cavities on the surface may exist a number of configurations capable of maintaining stable vapor embryos by comparison to the mirror polished surface. In the regime of nucleate boiling, roughness significantly enhanced heat transfer (shifting the curve to the left) indicating a significant increase in the number of active sites at a given heat flux. Messina and Park (1981) reported similar boiling augmentation of R-113 on a copper surface etched with jagged pits or sanded with fine sandpaper. Increased roughness lowered the superheat at CHF, but did not alter the magnitude of CHF noticeably, in contrast to the investigations of Messina and Park (1981), who detected a significant increase in CHF with increased roughness. The surface treatment for the remainder of the surfaces discussed in this paper was vapor blasting. It was chosen for its advantages in controlling hysteresis and augmenting nucleate boiling heat transfer.

Effects of Artificial Cavities. A smooth vapor blasted surface modified by three unique drilled cavity patterns revealed the inability of large cavities to retain vapor embryos of FC-72. However, some amount of control over the propagation of the boiling area can be exercised by proper placement of the cavities. Figure 9 shows that the incipience temperature was most reduced for the inclined array of cavities. Tests were run after $\Delta t^* = 8$ h. Nucleation began near the upper edge of all three enhanced surfaces, not at the cavities, indicating that no moderately sized vapor embryo existed within the drilled holes. As with the smooth vapor blasted surface, the gradual growth of A^* was from top to bottom with increasing flux except for the vertically arrayed surface. Following incipience on the vertical cavity surface, the top cavity began to boil, releasing relatively large bubbles. These bubbles were sufficient in size to activate the hole immediately below it. Within 20 s at the same flux the entire vertical row and surrounding area were completely active, resulting in a 6.0°C surface temperature drop. The cavities of the horizontal and inclined array become active only as the front of the boiling patch passed over them. Despite their relative reluctance to become active before microscopic cavities when heat flux was increased, large cavities were the last to cease boiling as the flux was decreased. Similar to the trend seen for natural convection, nucleate boiling and CHF were most enhanced by the inclined array of artificial cavities. The magnitude of CHF and the associated superheat for the horizontal and vertical cavity arrays were almost identical to that of the plain (nondrilled) vapor blasted surface indicating that these particular cavity patterns had little or no effect on the formation of the vapor blanket. However, the inclined array was successful at increasing the maximum flux by 25 percent through enhancement of the boiling prior to the onset of transition to film boiling. In contrast, experiments with very shallow pits on a mirror surface by Messina and Park (1981) suggest an optimum cavity size and distribution can enhance CHF markedly. Further experimentation with placement and geometry of artificial cavities may result in more precise control of the growth of the active boiling area and enhancement of CHF.

Figure 10 shows a comparison of natural convection data for all the flat surfaces including those with artificial cavities. Except for the inclined cavity array, data for all the flat surfaces seem to follow a unique convection coefficient correlation indicating the weak effect surface roughness, vertical

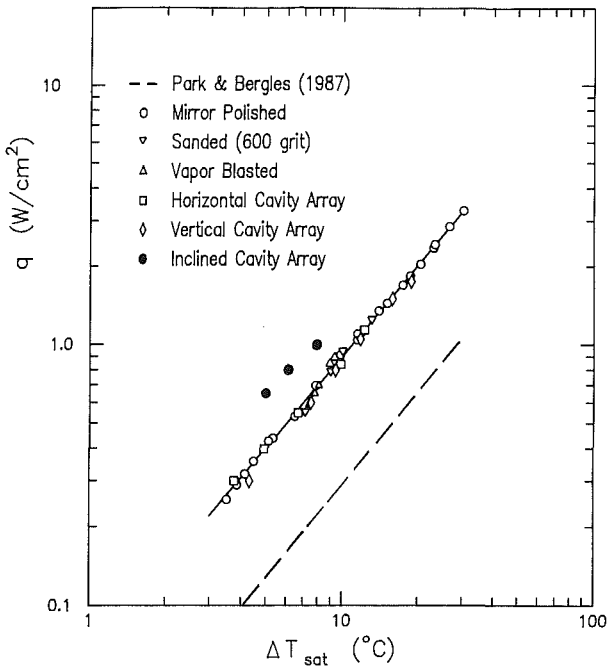

Fig. 10 Comparison of present natural convection data with the correlation of Park and Bergles (1987)

cavities, and horizontal cavities have on natural convection. Inclined cavities showed some enhancement over the other surfaces due, perhaps, to enhanced turbulent activity the orientation of these cavities imposes on vertical fluid motion near the upstream edge of the thermal boundary layer. Also shown in Fig. 10 is the empirical correlation

$$\mathrm{Nu}_c = 0.906\left[1+\frac{0.011}{(W/W_\infty)^{3.965}}\right]^{0.2745}\mathrm{Ra}_c^{*\delta} \tag{4}$$

where

$$\delta = 0.184\left[1+\frac{2.64\times10^{-5}}{(W/W_\infty)^{9.248}}\right]^{-0.0362}$$

$$W_\infty = 70\ \mathrm{mm}$$

developed by Park and Bergles (1987) for natural convection from a small foil heater of height H and width W (typical of electronic chip size) in R-113. The large deviation between the present data and the Park and Bergles correlation can be explained, in part, by the differences in thermal properties between the fluids used in the two studies, and by the fundamental differences in measuring the heat transfer coefficient. Unlike the isothermal surface condition of the present study, Park and Bergles utilized a thin foil heater, which imposed a constant heat flux boundary, and the wall temperature was measured only at the vertical center of the foil. Differences between the two correlations may also be traced back to the different three-dimensional pool geometries surrounding the two types of heater. These geometric effects are believed to influence the natural circulation pattern in the vicinity of the heater.

Effects of Low-Profile Surface Structures. Figures 11 and 12 show that low-profile microfin, microstud, and inclined microgroove structures significantly augment nucleate boiling heat transfer at the expense of increased incipience excursion. Although natural convection for the microfin is more efficient than for the smooth surface (due to the more than doubled surface area), still greater enhancement is caused by the development of *multiple boundary layers* on the lower edges of the microstud structure. Another advantage of the microstud geometry is related to the stagnation of the induced flow caused by the downward-facing sides of the studs. Ap-

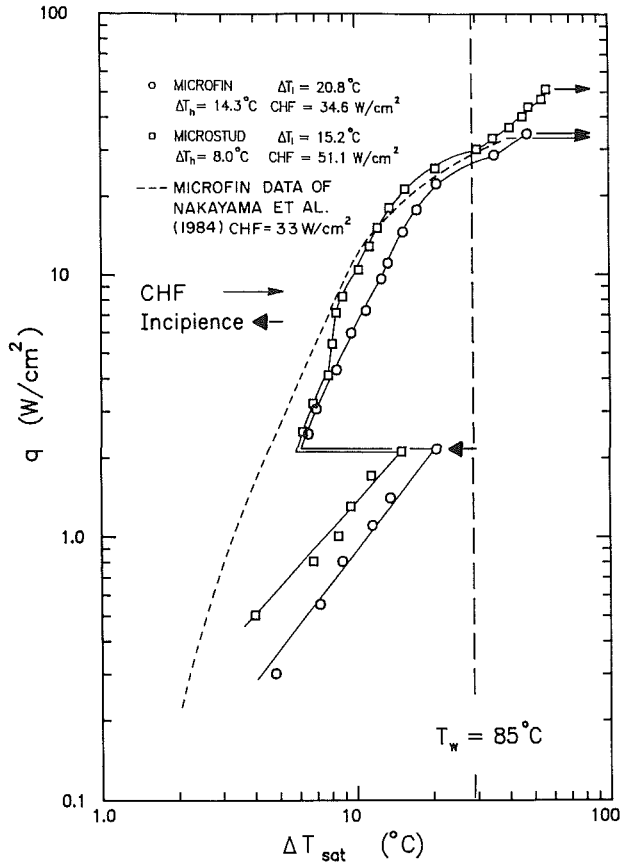

Fig. 11 Effect of microfin and microstud structures on the boiling curve

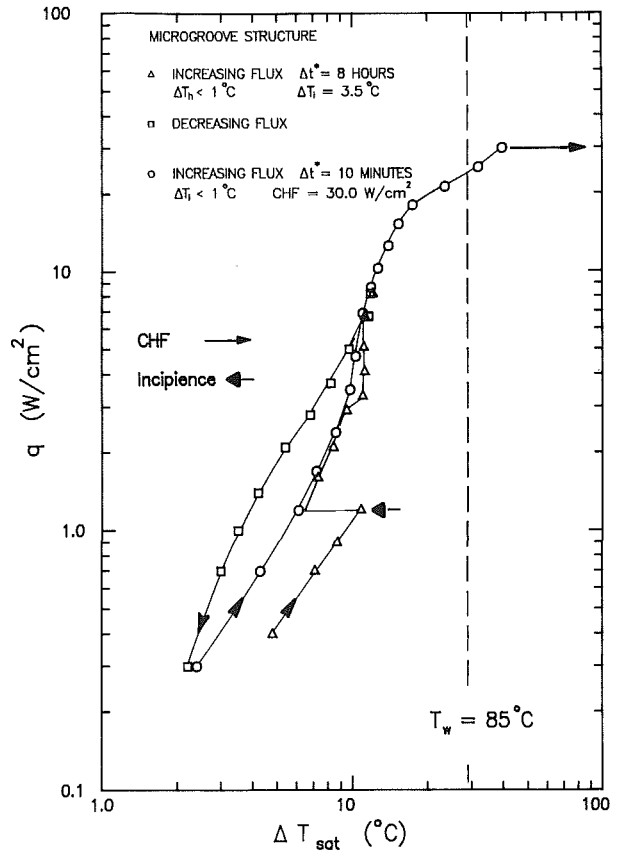

Fig. 12 Effect of inclined microgrooves on the boiling curve

parently the flow is slowed down allowing the liquid to be warmed to a temperature more favorable for activation of a vapor embryo. This effect is most clearly shown in the 5.6°C decrease in incipience temperature for the microstud compared to the microfin surface.

Incipience on the microfin and microstud were accompanied by 14.3 and 8.0°C of incipience excursion, respectively, as large portions of the chips rapidly activated. The quick growth of the boiling patch was caused by the growing bubbles' tendency to move downward along the surface through a combination of attachment to the neighboring studs and dryout of the area between the fins. The extreme levels of boiling enhancement associated with these structures will require significantly higher natural convection heat transfer coefficients to close the gap between the pre-incipience and post-incipience temperatures at typical values of incipient heat flux. Also shown in Fig. 11 are the data obtained by Nakayama for a similar microfin geometry oriented horizontally facing upward. The CHF values are close (33 versus 34.6 W/cm^2) but the horizontal orientation appears to enhance the nucleate boiling heat transfer slightly. However, the microstud surface resulted in a much higher CHF value of 51.1 W/cm^2. Comparison of the incipience performance of the two orientations is difficult since the Δt^* values of Nakayama's experiments were not reported; however, data taken with the vertical microfin after a short Δt^* period (10 min) display low incipience flux and temperature.

Multiple traverses of the inclined microgroove surface boiling curve (Fig. 12) show the dependence of curve hysteresis on Δt^*. The incipience temperature was further depressed compared to the microstud surface since stagnant pockets of warmed fluid were trapped within the grooves. The irregular shape of the inclined microgroove nucleate boiling curve is believed to be a product of the bubble activation pattern. As the initial bubble grew, they coalesced together very rapidly and activated the entire surface of the groove. The initial boiling from the uppermost groove was passed down to the next two grooves similar to the migration of activation seen with the vertical array of artificial cavities. The sudden jump in A^* resulted in a 3.5°C surface temperature drop. Further activation was more gradual as flux was increased to the fully developed region. Decreasing the heat flux revealed an additional augmentation in the heat transfer at lower power levels compared to the case of increasing heat flux as the majority of the grooves remained boiling. Very low values of the boiling cessation flux and superheat were echoed by low values at incipience as the heat flux was increased after 10 min of nonboiling. The third traverse of the boiling curve fell between the first two until a convergence at the point of fully developed boiling ($q \approx 8$W/cm^2) occurred. The lack of protruding structures to influence the onset of burnout explains the moderate peak flux, CHF = 39.8 W/cm^2.

The microfin and microstud surfaces experienced similar trends to the boiling curve when subjected to multiple traverses of the boiling curve with Δt^* first fixed at 8 h and then at 10 min.

Summary

This study was conducted to gain a good understanding of the trends associated with pool boiling of FC-72 on a vertical surface. Specific conclusions for the design of direct immersion electronic cooling packages are as follows:

1 Common incipience theories based on cavity radius do not apply to highly wetting fluids such as FC-72. Incipience is sensitive to the value of the effective radius of vapor embryos existing within the surface; however, that radius may be a very complex function of surface microstructure and the temperature/pressure history prior to boiling.

2 Increasing the nonboiling waiting period appears to increase the incipience temperature and incipient excursion.

3 Artificial cavities on the order of 0.3 mm diameter are ineffective in lowering the incipience temperature, enhancing nucleate boiling, or increasing CHF.

4 Microstructures significantly shift the boiling curve toward lower superheats while increasing the incipience excursion.

5 The maximum heat flux is a function of surface geometry and orientation but independent of initial conditions, surface roughness, or the presence of large artificial cavities. The microstud surfaces provided CHF values in excess of 50 W/cm^2.

Acknowledgments

Support of this work by a grant from the IBM Corporation is gratefully acknowledged. The assistance of Mr. Richard C. Chu, Mr. Robert E. Simons, and Dr. Dereje Agonafer of IBM is appreciated. The authors also thank Mr. R. D. Danielson of the Industrial Chemical Products Division of 3M for providing fluid samples and technical information on the test fluid.

References

Bar-Cohen, A., and Simon, T. W., 1986, "Wall Superheat Excursions in the Boiling Incipience of Dielectric Fluids," *Heat Transfer in Electronic Equipment*, A. Bar-Cohen, ed., ASME HTD-Vol. 57, pp. 83–94.

Blander, M., and Katz, J. L., 1975, "Bubble Nucleation in Liquids," *AIChE Journal*, Vol. 21, pp. 833–848.

Danielson, R. D., Tousignant, T., and Bar-Cohen, A., 1987, "Saturated Pool Boiling Characteristics of Commercially Available Perfluorinated Inert Liquids," *Proceedings of the 1987 ASME–JSME Thermal Engineering Joint Conference*, Honolulu, HI, Vol. 3, pp. 419–430.

Davis, E. J., and Anderson, G. H., 1966, "The Incipience of Nucleate Boiling in Forced Convection Flow," *AIChE Journal*, Vol. 12, pp. 774–780.

Han, C. Y., and Griffith, P., 1965, "The Mechanism of Heat Transfer in Nucleate Pool Boiling," *International Journal of Heat and Mass Transfer*, Vol. 8, pp. 887–903.

Hsu, Y. Y., 1962, "On the Size Range of Active Nucleation Cavities on a Heating Surface," ASME Journal of Heat Transfer, Vol. 84, pp. 207–216.

Hui, T. O., amd Thome, J. R., 1985, "A Study of Binary Mixture Boiling: Boiling Site Density and Subcooled Heat Transfer," *International Journal of Heat and Mass Transfer*, Vol. 28, pp. 919–928.

Marto, P. J., and Lepere, V. J., 1982, "Pool Boiling Heat Transfer From Enhanced Surfaces to Dielectric Fluids," ASME Journal of Heat Transfer, Vol. 104, pp. 292–299.

Messina, A. D., and Park, E. L., 1981, "Effects of Precise Arrays of Pits on Nucleate Boiling," *International Journal of Heat and Mass Transfer*, Vol. 24, pp. 141–145.

Nakayama, W., Nakajima, T., and Hirasawa, S., 1984, "Heat Sink Studs Having Enhanced Boiling for Cooling of Microelectronic Components," ASME Paper No. 84-WA/HT-89.

Park, K. A., and Bergles, A. E., 1985, "Heat Transfer Characteristics of Simulated Microelectronic Chips Under Normal and Enhanced Conditions," Iowa State College of Engineering Interim Technical Report HTL-35, submitted to IBM Data Systems Division.

Park, K. A., and Bergles, A. E., 1986, "Boiling Heat Transfer Characteristics of Simulated Microelectronic Chips With Detachable Heat Sinks," *Proceedings of the Eighth International Heat Transfer Conference*, San Francisco, CA, Vol. 4, pp. 2099–2104.

Park, K. A., and Bergles, A. E., 1987, "Natural Convection Heat Transfer Characteristics of Simulated Microelectronic Chips," ASME Journal of Heat Transfer, Vol. 109, pp. 90–96.

Ramadhyani, S., and Incropera, F. P., 1987, "Forced Convection Cooling of Discrete Heat Sources With and Without Surface Enhancement," *Proceedings of the International Symposium on Cooling Technology for Electronic Equipment*, Honolulu, HI, pp. 249–264.

Sabersky, R. H., and Gates, C. W., 1955, "On the Start of Nucleation in Boiling Heat Transfer," *Jet Propulsion, Journal of the American Rocket Society*, Vol. 25, pp. 67–70.

Tuckerman, D. B., and Pease, R. F. W., 1981, "High-Performance Heat Sinking for VLSI," *Electronic Device Letters*, EDL-2, pp. 126–129.